Knockout of the LRRC26 subunit reveals a primary role of LRRC26-containing BK channels in secretory epithelial cells

Chengtao Yang[a], Vivian Gonzalez-Perez[a], Taro Mukaibo[b,c], James E. Melvin[b], Xiao-Ming Xia[a], and Christopher J. Lingle[a,1]

[a]Department of Anesthesiology, Washington University School of Medicine, St. Louis, MO 63110; [b]Secretory Mechanisms and Dysfunction Section, National Institute of Dental and Craniofacial Research, National Institutes of Health, Bethesda, MD 20892-4320; and [c]Department of Oral Reconstruction and Rehabilitation, Kyushu Dental University, Kitakyushu, Fukuoka 803-8580, Japan

Edited by Ramon Latorre, Centro Interdisciplinario de Neurociencias de Valparaíso, Facultad de Ciencias, Universidad de Valparaíso, Valparaiso, Chile, and approved March 27, 2017 (received for review February 22, 2017)

Leucine-rich-repeat-containing protein 26 (LRRC26) is the regulatory γ1 subunit of Ca^{2+}- and voltage-dependent BK-type K^+ channels. BK channels that contain LRRC26 subunits are active near normal resting potentials even without Ca^{2+}, suggesting they play unique physiological roles, likely limited to very specific cell types and cellular functions. By using *Lrrc26* KO mice with a β-gal reporter, *Lrrc26* promoter activity is found in secretory epithelial cells, especially acinar epithelial cells in lacrimal and salivary glands, and also goblet and Paneth cells in intestine and colon, although absent from neurons. We establish the presence of LRRC26 protein in eight secretory tissues or tissues with significant secretory epithelium and show that LRRC26 protein coassembles with the pore-forming BK α-subunit in at least three tissues: lacrimal gland, parotid gland, and colon. In lacrimal, parotid, and submandibular gland acinar cells, LRRC26 KO shifts BK gating to be like α-subunit-only BK channels. Finally, LRRC26 KO mimics the effect of SLO1/BK KO in reducing [K^+] in saliva. LRRC26-containing BK channels are competent to contribute to resting K^+ efflux at normal cell membrane potentials with resting cytosolic Ca^{2+} concentrations and likely play a critical physiological role in supporting normal secretory function in all secretory epithelial cells.

BK channels | LRRC26 | secretory epithelium | salivary glands | SLO1

Large-conductance, voltage- and Ca^{2+}-regulated BK-type channels are widely expressed proteins, found not only in excitable cells, such as neurons, muscle, and endocrine cells, but also nonexcitable cells, including salivary (1) and lacrimal gland (2) acinar cells, and colonic crypt cells (3). Given the almost ubiquitous expression of BK channels among cells that play quite distinct physiological roles, it is particularly important to define the specific properties of BK channels in a given cell type and determine what the specific physiological role played by BK channels in a given cell may be. A hallmark of BK channels is their dual regulation by both membrane voltage and cytosolic Ca^{2+} (4), both properties embedded within the tetramer of pore-forming α-subunits of each BK channel (5). However, the specific range of voltages over which a BK channel is active at a given Ca^{2+} concentration is markedly dependent on the identity of regulatory subunits that can coassemble with the α-subunit in the mature channel complex. Of the two families of known BK regulatory subunits, β (6–11) and γ (12–14), an important feature of many of these subunits is the ability to shift the range of activation voltages at a given Ca^{2+}. Although there is growing information about the loci of expression and functional roles of BK channels containing specific β-subunits (15), much less is known about those BK channels containing the γ1 (LRRC26, leucine-rich-repeat-containing subunit 26) subunit. However, LRRC26 is particularly fascinating because it causes the largest shift in BK gating (approximately −120 mV) of any known non–pore-forming regulatory subunit, resulting in BK channels that can be activated near normal cell resting potentials, even in the absence of any elevation of cytosolic Ca^{2+} (12). Naturally, one wonders, where are LRRC26-containing BK channels found and what is their fundamental physiological role?

LRRC26 was originally identified in several cancer cell lines and termed cytokeratin-associated protein in cancers (CAPC) (16). Subsequently it was shown to be a regulatory subunit of BK channels (12), later defined as γ1 (14). LRRC26 accounts for the large shift in BK activation toward negative potentials found in LNCaP prostate tumor cells (17), whereas similar shifts in BK gating attributable to LRRC26 have also been observed in mouse parotid gland acinar cells (18, 19). In other cases where the presence of LRRC26 has been suggested, definitive evidence of BK channels with properties consistent with the presence of LRRC26 is lacking. The uniquely distinct kind of BK channel created by the presence of LRRC26 suggests that such channels likely play unique physiological roles distinct from those played by BK channels in excitable cells.

As a step toward a more systematic answer to this issue, here we describe a *Lrrc26* KO mouse, in which a *lacZ* reporter gene replaces the *Lrrc26* allele. Through the use of qRT-PCR and β-gal staining, the results demonstrate detectable *Lrrc26* promoter activity only in secretory epithelial cells across a variety of tissues, with weak *Lrrc26* message and no promoter activity in any known type of excitable cell, including neurons and smooth muscle. Based

Significance

Ca^{2+}- and voltage-regulated K^+ channels (termed BK channels) are expressed in a diverse variety of cells, playing distinct physiological roles often defined by cell-specific regulatory subunits. Here, genetic deletion of one particular regulatory subunit, LRRC26, reveals that LRRC26-containing BK channels are found, perhaps exclusively, in secretory epithelial cells, including salivary glands, airways, and gastrointestinal tract. Such cells mediate fluid, peptide, and mucus secretion, influencing digestion, airway function, gut resistance to infection, and lactation. The absence of LRRC26 in secretory epithelial cells renders BK channels inactive during normal physiological conditions and alters ion efflux from salivary gland. LRRC26-containing BK channels are critical for normal ionic flux in secretory epithelial cells, likely impacting on a variety of epithelial cell pathologies.

Author contributions: C.Y., V.G.-P., T.M., J.E.M., and C.J.L. designed research; C.Y., V.G.-P., T.M., and X.-M.X. performed research; X.-M.X. contributed new reagents/analytic tools; C.Y., V.G.-P., T.M., J.E.M., and C.J.L. analyzed data; and C.Y. and C.J.L. wrote the paper.

The authors declare no conflict of interest.

This article is a PNAS Direct Submission.

[1]To whom correspondence should be addressed. Email: clingle@morpheus.wustl.edu.

This article contains supporting information online at www.pnas.org/lookup/suppl/doi:10.1073/pnas.1703081114/-/DCSupplemental.

on candidate tissues with high message levels, we confirmed the presence of LRRC26 protein in various tissues. In the three tissues with the most abundant protein: parotid gland, lacrimal gland, and colon, we demonstrate coimmunoprecipitation (co-IP) of LRRC26 and SLO1. Furthermore, using lacrimal, parotid cells, and submandibular gland acinar cells, we show that LRRC26 KO results in large positive shifts in the activation range of BK channels. Finally, we show that the absence of LRRC26 is sufficient to account for the effects of SLO1 KO in reducing potassium secretion in saliva from mouse salivary glands. These results suggest that LRRC26-containing BK channels are suited to a specific role in secretory epithelial cells, contributing to maintenance of normal fluid and electrolyte secretion.

Results

Survey of Potential Loci of Expression of *Lrrc26* Message. To provide a general overview of tissues likely to express LRRC26 protein, we used quantitative RT-PCR to test for *Lrrc26* message abundance relative to β-actin and compared this to expression levels of the *Kcnma1* (*Slo1*) message for the BK pore-forming subunit. In *SI Appendix*, Fig. S1*A*, loci of expression are grouped by general similarity of function, e.g., neuronal tissues, glandular tissues, and so on. Results for different tissues were also plotted in rank order of detected *Lrrc26* message (*SI Appendix*, Fig. S1*B*). Of 38 tested mouse tissues, lacrimal, parotid, and submandibular glands show the highest *Lrrc26* message abundance. In contrast, hippocampus, cerebral cortex, liver, adrenal, and heart ventricle show the lowest levels of *Lrrc26* message expression, more than 500-fold lower than observed in tissues most enriched in *Lrrc26* message. It is worth noting that, in intestine, there is a trend for *Lrrc26* message to increase distally (duodenum, 0.0035 ± 0.0010 < jejunum, 0.0041 ± 0.0007 < ileum, 0.0071 ± 0.0017 < colon, 0.0152 ± 0.0038, values normalized to β-actin). Also, *Lrrc26* message in vagina is markedly increased during pregnancy.

LRR26 Protein Can Be Readily Detected in Most Native Tissues with High Lrrc26 Message. To facilitate definition of the loci of expression of LRRC26 protein, we used LRRC26 KO mice obtained from the Knockout Mouse Program (KOMP) (University of California-Davis) in which a *lacZ* reporter gene replaces the full-length *Lrrc26* coding sequence (*SI Appendix*, Fig. S2*A*), along with a custom polyclonal antibody made to an epitope on the cytosolic C terminus of mouse LRRC26 (*Materials and Methods*). We first confirmed successful disruption of the *Lrrc26* gene via PCR of mouse tails (*SI Appendix*, Fig. S2*B*). Subsequently, because both our qRT-PCR results and earlier results suggest LRRC26 protein is present in prostate (12, 20), membrane proteins were prepared from isolated prostate glands of *wt* and *Lrrc26*$^{-/-}$ mice and the LRRC26 protein was concentrated by immunoprecipitation (IP) with the rabbit anti-LRRC26 antibody. The LRRC26-IP products were then blotted with the same antibody (*SI Appendix*, Fig. S2*C*). Mouse LRRC26 protein has 331 amino acids and, according to the sequence, is predicted to be about 36 kDa. It has a potential N-linked glycosylation site at N56 in the extracellular domain. After the removal of the N-terminal signal peptide, the mature LRRC26 is predicted to be about 33 kDa. In the Western blot (WB) of LRRC26-IP products from prostate, a single band (~40 kDa) is seen only in WT sample and totally absent in KO sample (*SI Appendix*, Fig. S2*C*). After PNGase F treatment to remove N-linked oligosaccharides, the resulting deglycosylated product is shifted to ~35 kDa, generally consistent with the expected molecular weight (MW) of mouse LRRC26. Together these results confirm that the bands detected by the rabbit anti-LRRC26 Ab correspond to the LRRC26 protein. Because the MW of PNGase F-treated LRRC26 (35 kDa) is still somewhat larger than the predicted MW of the mature LRRC26 protein (33 kDa), it is possible that LRRC26 in mouse prostate has additional modifications other than N-linked glycosylation. The absence of LRRC26 protein in the *Lrrc26*$^{-/-}$ prostate confirms the successful deletion of the *Lrrc26* gene.

Using a similar sequential IP and WB strategy with the anti-LRRC26 Ab along with a comparison of tissues from *wt* and *Lrrc26*$^{-/-}$ mice, we next determined that LRRC26 protein could also be identified both in tissues with relatively high *Lrrc26* message levels, including lacrimal gland, parotid, and submandibular gland (Fig. 1*A*), and also tissues with lower Lrrc26 message levels, including trachea, mammary gland, and lung (Fig. 1*B*) and also colon and glandular stomach (Fig. 1*C*). LRRC26 protein could not be detected from membrane protein samples from the cerebellum (Fig. 1*C*).

We noticed that LRRC26 protein exhibited different forms in different tissues. In lacrimal gland and submandibular gland, LRRC26 migrated as a single band in Western blots as observed in the prostate samples. However, multiple LRRC26 bands were clearly observed in parotid, colon, trachea, and lung with the MW ranging from 38 kDa to 48 kDa. The results suggest that different tissues may exhibit differential posttranslational processing of LRRC26 protein or perhaps alternative splicing of *Lrrc26* message that has not as yet been reported. Although all bands were shifted to smaller sizes with PNGase F treatment, the number of bands and their relative densities appeared unchanged by deglycosylation. Similar to these observations, multiple bands of LRRC26 were reported from the human MDA-231 breast cancer cell line, both before and after PNGase F treatment (20), leading to the proposal that LRRC26 may contain modifications other than *N*-glycosylation. In this regard, the online O-linked glycosylation prediction server, NetOGlyc 4.0 (www.cbs.dtu.dk/services/NetOGlyc/), identifies nine Thr/Ser residues in the mouse LRRC26 sequence that are high likelihood candidates for O-GalNAc modifications, providing one possible explanation for tissue-specific differences in multiple LRRC26 bands. Both the basis for the tissue-specific diversity in molecular sizes of confirmed LRRC26 protein and the potential functional implications of such diversity may prove interesting topics for future work.

LRRC26 May Be Exclusively Expressed in Secretory Epithelial Cells. In the LRRC26 KO mice, the β-galactosidase reporter under control of the *Lrrc26* promoter provides another tool to reveal potential loci of *Lrrc26* message expression and offers the advantage that the cellular loci of β-gal activity can potentially be visualized. To evaluate loci of *Lrrc26* promoter activity, 20- to 25-μm sections were prepared from various tissues and incubated with the Bluo-Gal substrate. Incubation conditions that were required to reveal β-gal reaction product varied appreciably among tissues (*Materials and Methods*), perhaps reflecting cell-specific differences in regulation of promoter activity or differences in success in tissue permeation with substrate. Despite variations in optimal reaction conditions among cells, direct side-by-side comparison of *wt* vs. KO tissues provides assurance regarding the specificity of any observed reaction product. In all tissues for which a positive β-gal reaction product is observed, the positive staining is seen only in likely epithelial cells.

Positive Bluo-Gal staining is readily observed in acinar epithelial cells in lacrimal gland and salivary glands. Fig. 2 *A–D* shows sections from *wt* (*Left*) and LRRC26 KO (*Right*) glandular tissues reacted for Bluo-Gal. All sections are counterstained with eosin. Lower gain sections showing most of each gland are displayed in *SI Appendix*, Fig. S3 *A–D*. Even at the shortest tested Bluo-Gal incubation times (1–2 h), Bluo-Gal staining in the lacrimal gland exceeded other tissues (Fig. 2*A*), generally consistent with an abundance of message (*SI Appendix*, Fig. S1) and protein (Fig. 1). Strong staining is observed throughout the acinar cells in the lacrimal gland KO section, but not the *wt* section. Although parotid had a similar level of *Lrrc26* message (*SI Appendix*, Fig. S1) and protein (Fig. 1) compared with lacrimal gland, dark blue staining in LRRC26 KO parotid sections required about 24 h of

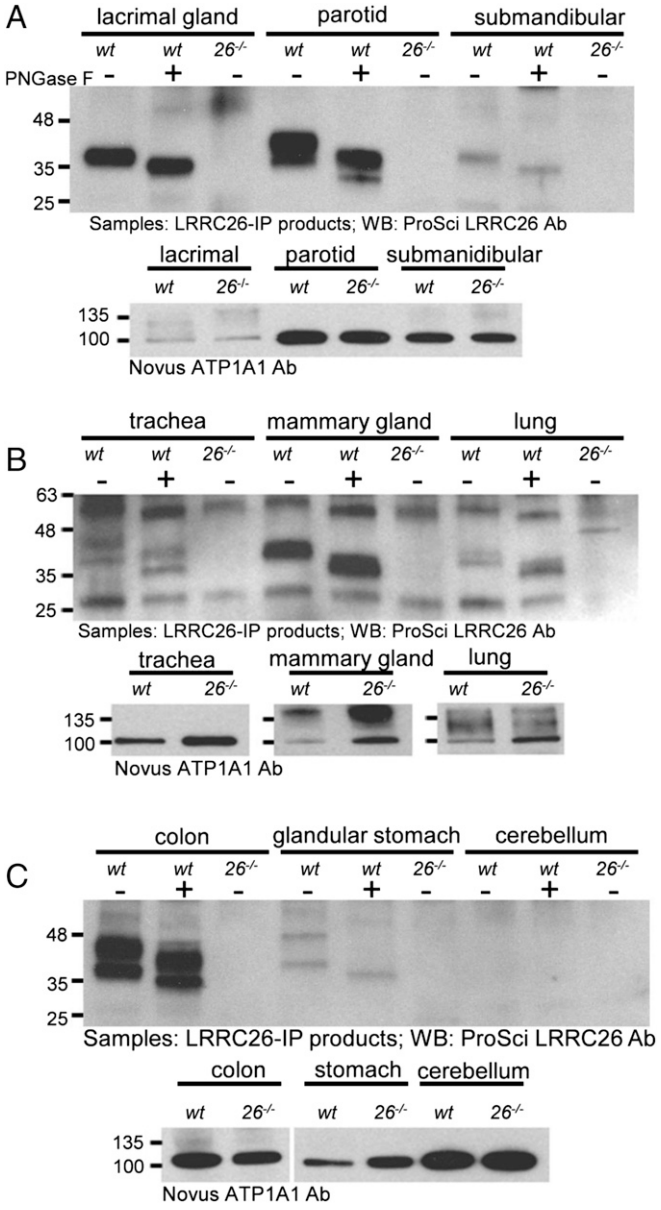

Fig. 1. Detection of LRRC26 protein in *Lrrc26* message-rich mouse tissues. (*A*) Across the *Top*, membrane protein samples were prepared from each of the indicated tissues and immunoprecipitated with the LRRC26 polyclonal Ab. Samples were split to allow treatment with (+) or without (–) PNGase F, and also to allow detection of protein levels in the sample (across the *Bottom*). A Novus Anti-Na^+/K^+ATPaseA1 (ATP1A1) Ab was used to determine that similar amounts of protein from *wt* and LRRC26 KO samples were loaded. Protein amounts (in milligrams) used for LRRC26-IP product preparation were 0.1, 0.2, and 0.8 for lacrimal, parotid, and submandibular glands. For ATP1A1 detection, 75, 17, and 27 μg membrane proteins were loaded in each case. (*B*) For trachea, lactating mammary gland, and lung, the membrane protein amounts used to generate IP product were 0.5, 3.7, and 1.5 mg, with 55, 86, and 83 μg of membrane protein used to monitor ATP1A1. (*C*) For colon, glandular stomach, and cerebellum, 1.5, 1.1, and 1.6 mg of membrane protein samples were used for the preparation of IP product in each lane, whereas 44, 71, and 1 μg of membrane proteins were loaded for detection of ATP1A1 for the same tissues.

incubation to develop, compared with 1–2 h for lacrimal gland, with Bluo-Gal staining in the parotid occurring in both acini cells and ducts (*SI Appendix*, Fig. S4 *A* and *B*). Unlike lacrimal and parotid glands, where serous acini are most dominant, the mouse submandibular gland contains exclusively seromucous cells interspersed with primarily granular duct cells. The submandibular KO sections exhibit strong positive Bluo-Gal staining (*SI Appendix*, Fig. S3*C*), which is most prominent in seromucous acini (Fig. 2*C*). Finally, in the sublingual gland, which contains primarily mucous cells, sections from the LRRC26 KO tissue exhibit strong positive Bluo-Gal straining (*SI Appendix*, Fig. S3*D* and Fig. 2*D*) comparable to that in the submandibular gland (*SI Appendix*, Fig. S3*C*). Staining in LRRC26 KO sections showing both sublingual and submandibular glands was more prominent after 24-h Bluo-Gal incubation time than after 2 h (*SI Appendix*, Fig. S4 *C* and *D*), but ductal cells in the *wt* submandibular gland also revealed some nonspecific darkening.

Positive Bluo-Gal staining was also observed in goblet cells and Paneth cells in the epithelium of small intestine (Fig. 2 *E* and *G* and *SI Appendix*, Fig. S3*E*) and colon (Fig. 2*F* and *SI Appendix*, Fig. S3*F*). The proportion of goblet cells among epithelial cell types increases caudally from duodenum (4%) to jejunum (6%) to ileum (12%) to distal colon (16%) (21). We found a qualitatively similar rostral-to-caudal increase of *Lrrc26* message from duodenum to colon in our qRT-PCR data (Fig. 1), raising the possibility that β-gal positive cells are goblet cells. Because goblet cells produce mucins, they can be visualized with the periodic acid-Schiff (PAS) staining method (22, 23). For both the small intestine (Fig. 2*E*) and the colon (Fig. 2*F*), tissue sections were therefore prepared with both Bluo-Gal staining and the PAS counterstain. In *wt* sections, PAS stained the mucin granules with magenta in the apical part of goblet cells, whereas in LRRC26 KO sections additional dark blue Bluo-Gal staining was observed in the narrow base of the same cells stained with PAS. This confirms that Bluo-Gal–stained cells in small intestinal villi and in colon are goblet cells. Furthermore, in the crypts of the small intestine, positive Bluo-Gal staining signals appeared not only in PAS^+ goblet cells, but also in PAS^+ Paneth cells (24) at the base of crypts (Fig. 2*G*). In the colon, positive Bluo-Gal activity is most prominent in the upper half of the colonic crypts.

Positive Bluo-Gal staining specific to sections from LRRC26 KO mice was also obvious in both the vomeronasal organ (VNO) (*SI Appendix*, Fig. S5 *A* and *B*) and conjunctiva of the eye (*SI Appendix*, Fig. S5 *C* and *D*). In the VNO, the PAS stain identifies the vomeronasal gland, also termed Jacobson's gland (25). In VNO sections from LRRC26 KO animals, the magenta signal of PAS staining colocalized with the dark blue signals from the β-gal reaction (*SI Appendix*, Fig. S5 *A* and *B*). Positive staining was also seen in the receptor-free epithelium of the VNO. Similarly, in the conjunctiva, Bluo-Gal staining (*SI Appendix*, Fig. S5*C*) appears to overlap with PAS staining (*SI Appendix*, Fig. S5*D*). In the conjunctiva, PAS staining identifies mucus-secreting goblet cells (26, 27).

Positive Bluo-Gal staining cells were also observed in epithelium of trachea (*SI Appendix*, Fig. S6*A*), bronchioles of the lung (*SI Appendix*, Fig. S6*B*), oviduct (*SI Appendix*, Fig. S6*C*), prostate (*SI Appendix*, Fig. S6*D*), uterus (*SI Appendix*, Fig. S6*E*), cervix, vagina (*SI Appendix*, Fig. S6*F*), and mammary gland of lactating females (*SI Appendix*, Fig. S6*G*). The epithelial layer exhibiting Bluo-Gal staining in cervix and vagina was markedly thickened during pregnancy (for cervix, *SI Appendix*, Fig. S7 *A* vs. *B*; for vagina, *SI Appendix*, Fig. S7 *C* vs. *D*). In both cervix (*SI Appendix*, Fig. S8*A*) and vagina (*SI Appendix*, Fig. S8*B*), this thickening is associated in part with prominent remodeling of Bluo-Gal positive columnar epithelial cells. Comparison of *wt* and $Lrrc26^{-/-}$ KO sections from lactating mammary gland at higher resolution (*SI Appendix*, Fig. S9) revealed staining in cells likely to line the alveoli and also those that contribute to lactiferous ducts.

Many tissues were entirely negative for Bluo-Gal reaction even with prolonged reaction times (*SI Appendix*, Fig. S10). These tissues included brain regions, pancreas, kidney, glandular stomach, spleen, bladder, vas deferens, cauda epididymis, aorta, and cerebral artery. The absence of a positive Bluo-Gal signal in the glandular

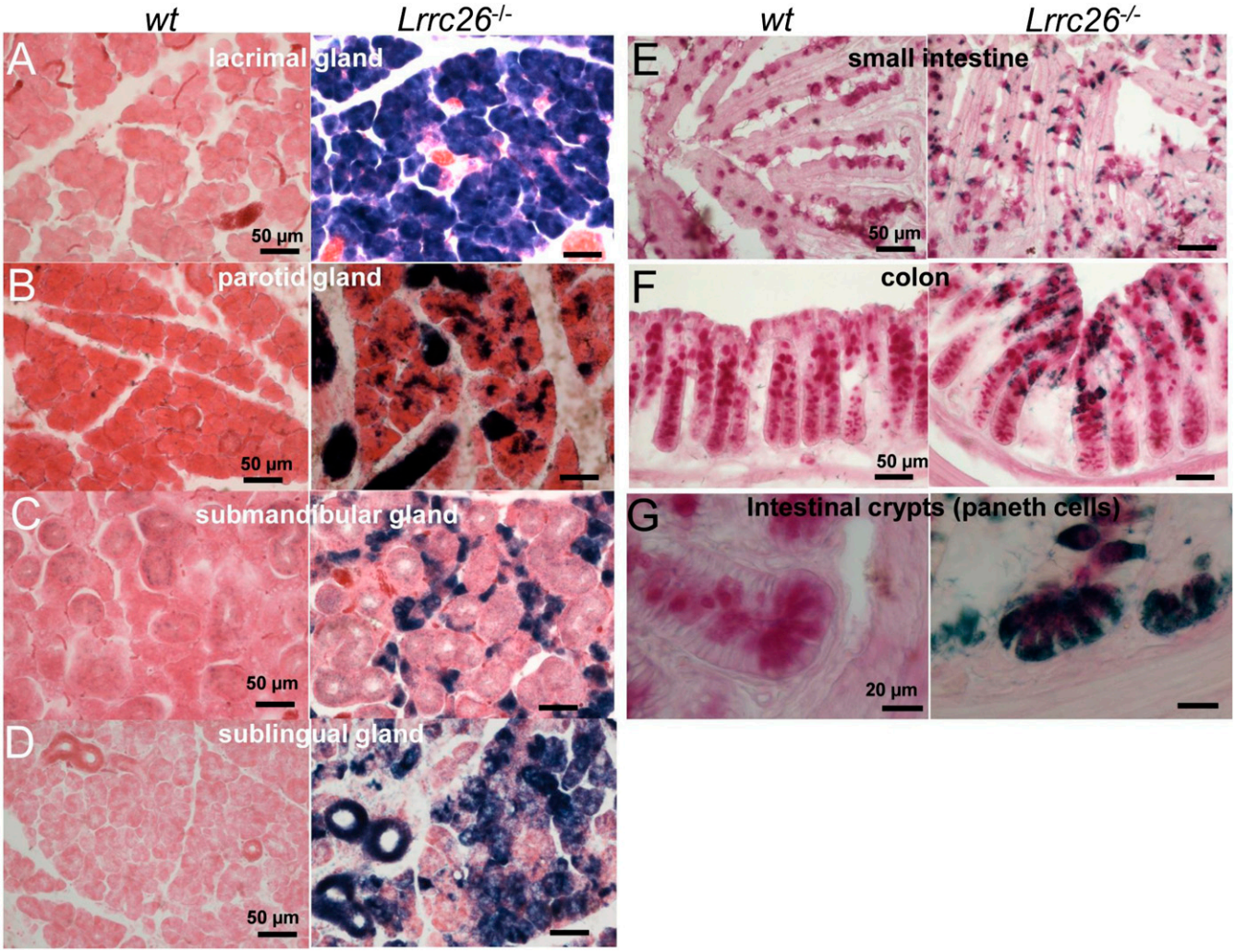

Fig. 2. Bluo-Gal staining is observed in glandular acinar cells and goblet and Paneth cells of gastrointestinal tract. In *A–D*, tissues were developed for Bluo-Gal staining and counterstained with eosin. (*A*) LRRC26 KO tissues show abundant Bluo-Gal reaction product throughout a lacrimal gland section that is absent in *wt* sections. (*B*) In parotid, Bluo-Gal reaction product (*Right*) is observed sparsely, but throughout acinar cells, whereas dense staining likely corresponds to intralobular and interlobular parotid ducts. (*C*) Bluo-Gal staining in submandibular gland is confined to cells likely to be seromucous acinar cells, whereas larger glandular duct cells display little if any staining. (*D*) Bluo-Gal staining in sublingual gland is distributed throughout acinar cells and ducts within the gland. In *E–G*, tissues were first processed with Bluo-Gal staining followed by a periodic acid-Schiff (PAS) reaction. (*E*) Goblet cells in villi of the small intestine are positive for PAS staining at the apical end corresponding to mucus granules and positive for Bluo-Gal staining at the basal end. (*F*) Crypts in the colon exhibit abundant PAS-positive cells, with the most superficial cells also enriched with Bluo-Gal staining. (*G*) Crypts of the small intestine reveal positive PAS staining and Bluo-Gal staining in Paneth cells and goblet cells.

stomach seems surprising, given that the qRT-PCR results suggest a high level of *Lrrc26* mRNA in this tissue (*SI Appendix*, Fig. S1), and that the weak presence of LRRC26 protein was confirmed by WB (Fig. 1). The absence of Bluo-Gal signal in acinar pancreas is also somewhat unexpected. Clearly, there is a wide range in the effectiveness of the Bluo-Gal staining protocol among tissues, even among those showing robust message levels, such as lacrimal and parotid glands. Spleen is another loci in which there is no obvious Bluo-Gal reaction, despite qRT-PCR data revealing a higher *Lrrc26* message level than in some other Bluo-Gal positive tissues (e.g., small intestine and vagina). Although reasons for the weaker than expected Bluo-Gal staining in some tissues are unclear, one possibility might be cell-specific variations in factors regulating promoter activity controlling β-gal expression.

Finally, with ovary, testis, and caput epididymis, sections from both *wt* and LRRC26 KO mice exhibited similar loci of darker coloration (*SI Appendix*, Fig. S11). Because of this nonspecific staining, we were unable to assess whether there is any *Lrrc26* promoter activity in these tissues, although the qRT-PCR estimates also confirm that *Lrrc26* message levels in these tissues are low.

LRRC26 Coassembles with SLO1 in Parotid Gland, Lacrimal Gland, and Colon. At least one important function of LRRC26 is to serve as a regulatory subunit of SLO1/BK channels (12, 14, 28). In addition to the profound functional effects of LRRC26 on BK channels, LRRC26 was shown to coimmunoprecipitate with SLO1 in LNCaP human prostate cancer cells (12). Here we selected three tissues: parotid gland, lacrimal gland, and colon, in which we were able to detect relatively abundant LRRC26 protein, to test whether LRRC26 coassembles with SLO1. First, membrane proteins were prepared from *wt*, *Slo1*$^{-/-}$, and *Lrrc26*$^{-/-}$ mice for the three tissues. The presence of SLO1 protein was then confirmed in *wt* and *Lrrc26*$^{-/-}$ membrane proteins, but not *Slo1*$^{-/-}$ proteins (Fig. 3 *A1*, *B1*, and *C1*). The protein samples were then checked for the presence of LRRC26 protein following an initial IP step with the

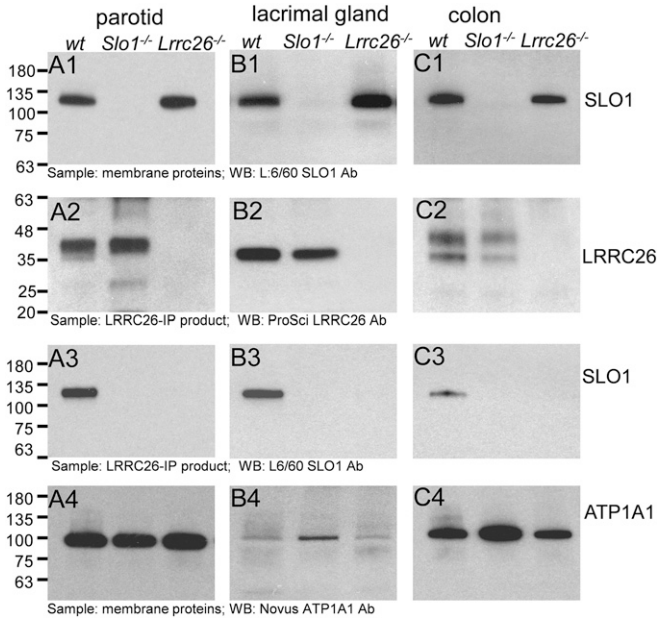

Fig. 3. Anti-LRRC26 antibody pulls down SLO1 protein in parotid, lacrimal gland, and colon. (*A*) Confirmation of LRRC26 association with SLO1 protein in mouse parotid. (*A1*) Total membrane proteins from parotid *wt*, *Slo1*$^{-/-}$, and *Lrrc26*$^{-/-}$ mice were blotted with anti-SLO1 Ab (L6/60, Antibodies, Inc.), identifying the SLO1 protein in *wt* and *Lrrc26*$^{-/-}$ mice, but not *Slo1*$^{-/-}$ mice. (*A2*) Proteins immunoprecipitated by the ProSci LRRC26 Ab were Western blotted, showing that LRRC26 is present in both *wt* and *Slo1*$^{-/-}$ *mice*, but not in the LRRC26 KO mice. (*A3*) Following immunoprecipitation of parotid membrane proteins with the LRRC26 Ab, SLO1 protein is identified in *wt* immunoprecipitated proteins, but not in *Slo1*$^{-/-}$ or *Lrrc26*$^{-/-}$ proteins. (*A4*) Aliquots of the parotid membrane protein preparations were blotted with a Na/K ATPase1A1 Ab to confirm that similar amounts of proteins were applied in all cases. (*B1*) Lacrimal gland total membrane proteins were blotted with the anti-SLO1 Ab. (*B2*) *wt* and *Slo1*$^{-/-}$, but not *Lrrc26*$^{-/-}$, lacrimal gland proteins contain LRRC26 protein. (*B3*) SLO1 protein is found in lacrimal gland membrane proteins immunoprecipitated with the LRRC26 Ab. (*B4*) Aliquots of lacrimal gland membrane proteins were blotted for ATP1A1. Note the markedly lower amounts of ATP1A1 in lacrimal gland, compared with parotid. (*C1–C4*) Slo1 protein in colon is also immunoprecipitated with the LRRC26 Ab.

LRRC26 polyclonal Ab, confirming the presence of LRRC26 protein in both *wt* and *Slo1*$^{-/-}$ proteins from all three tissues, but not in *Lrrc26*$^{-/-}$ proteins (Fig. 3 *A2*, *B2*, and *C3*). Subsequently, the LRRC26-IP products were blotted with the SLO1 Ab, indicating that SLO1 immunoprecipitates with LRRC26, but only in *wt* protein samples, and not in the samples from *Slo1*$^{-/-}$ or *Lrrc26*$^{-/-}$ mice (Fig. 3 *A3*, *B3*, and *C3*). For each tissue, an Ab to Na^+/K^+ATPase1A1 was used to confirm that similar amounts of proteins were applied (Fig. 3 *A4*, *B4*, and *C4*). The coassembly of LRRC26 with SLO1 in parotid gland, lacrimal gland, and colon supports the view that LRRC26 is a BK regulatory subunit in these tissues and predicts that BK gating will be shifted leftward in these cells.

LRRC26 KO Abolishes the Profound Leftward Activation Range of BK Currents in Cells from the Lacrimal, Parotid, and Submandibular Glands. Native cell BK currents that display functional properties consistent with the presence of SLO1 α and LRRC26 subunits have, to date, been clearly demonstrated only in prostate tumor cells (12, 17), parotid (18, 29), and submandibular (30, 31) gland cells. To confirm the consequences of LRRC26 KO on BK channel function in cells likely to express LRRC26, we used lacrimal, parotid, and submandibular dissociated acinar cells. For each gland, cells were acutely dissociated and whole-cell patch-clamp recordings were obtained with physiological K^+ gradients to compare currents in *wt* and LRRC26 KO cells. Because earlier work on parotid BK currents revealed some reduced sensitivity to the BK-specific inhibitor, iberiotoxin (32), and the β4 regulatory subunit of BK channels confers reduced iberiotoxin sensitivity on BK channels (33), we also examined currents in β4 KO parotid cells. In all cases, the pipette solution contained buffered 250 nM Ca^{2+}, which should produce minimal activation of any IK1 current present in such cells, while allowing robust voltage- and time-dependent BK activation. In *wt* lacrimal gland cells, depolarizing voltage steps result in activation of a time- and voltage-dependent outward current (Fig. 4*A1*), with appreciable activation even at voltages negative to 0 mV. In contrast, in lacrimal cells from the LRRC26 KO animals, even voltage steps to +100 mV produce minimal current activation (Fig. 4*A2*). KO of the BK β4 subunit does not appear to alter the lacrimal gland BK current properties (Fig. 4*A3*). Currents activated by identical protocols but in cells from the parotid gland exhibited almost identical properties. In *wt* cells, time- and voltage-dependent currents were activated at voltages negative to 0 mV (Fig. 4*B1*), whereas in LRRC26 KO cells, steps to +100 mV barely activated any current (Fig. 4*B2*), with no obvious effect of β4 subunit KO (Fig. 4*B3*). Currents obtained from submandibular acinar cells also showed robust activation in *wt* cells at voltages where little current was activated in LRRC26 KO cells (*SI Appendix*, Fig. S12*A*). Conductance vs. voltage (GV) curves generated from tail currents showed that KO of the LRRC26 subunit resulted in an ∼145 mV rightward gating shift for lacrimal gland cells (Fig. 4C), a rightward 120 mV gating shift in the parotid acinar cells (Fig. 4*D*), and a rightward 145 mV gating shift in the submandibular acinar cells (*SI Appendix*, Fig. S12*B*). The magnitude of the shift in gating with or without LRRC26 is consistent with the known effects of LRRC26 subunit when it is heterologously expressed with BK α-subunits (12, 28). Similarly, comparison of BK single channel activity in inside-out patches from *wt* and LRRC26 KO parotid gland cells reveals a similar gating shift to that observed in whole-cell recordings (*SI Appendix*, Fig. S13). In parotid cells (Fig. 4 *E* and *F*) cells, the time- and voltage-dependent currents were almost completely inhibited by either 5 mM tetraethylammonium (TEA) or 100 nM paxilline both in *wt* and LRRC26 KO cells. These sensitivities confirm that the currents both in *wt* and *Lrrc26*$^{-/-}$ cells are BK currents (Fig. 4*G*). Together these properties identify these currents as BK current and establish that LRRC26 is the critical partner of the BK pore-forming subunits that is essential for the left-shifted gating range in lacrimal, parotid, and submandibular gland acinar cells.

For the set of parotid cells, we observed no differences in average cell capacitance, BK current density, or IK current density (taking the leak current at −30 mV as an indication of IK) (*SI Appendix*, Fig. S14*A*). Given that β4 might have effects on channel kinetics that might not be revealed solely by examination of GV curves, we also measured activation time constants for *wt*, β4 KO, and LRRC26 KO parotid cells. No differences were observed between *wt* and β4 KO cells (*SI Appendix*, Fig. S14*B*), whereas activation time constants in LRRC26 KO parotid cells were slower at all voltages.

LRRC26 KO Reproduces the Effect of SLO1 KO in Reducing the Concentration of K^+ in Parotid and Submandibular Gland Salivary Secretions. Bulk saliva largely reflects contributions of secretion from three distinct paired salivary glands, the parotid, the submandibular, and the sublingual. The saliva composition varies to some extent among each gland type, differing in the extent to which glands that are largely composed of serous cells primarily secrete fluid and electrolytes or mucous cells that also secrete large amounts of glycosylated proteins such as mucins. An assay previously used to examine the role of KO of SLO1 α-subunits on salivary gland function is to monitor the salt composition of saliva collected either via an in vivo assay of parotid or submandibular glands or via an ex vivo assay of isolated, perfused

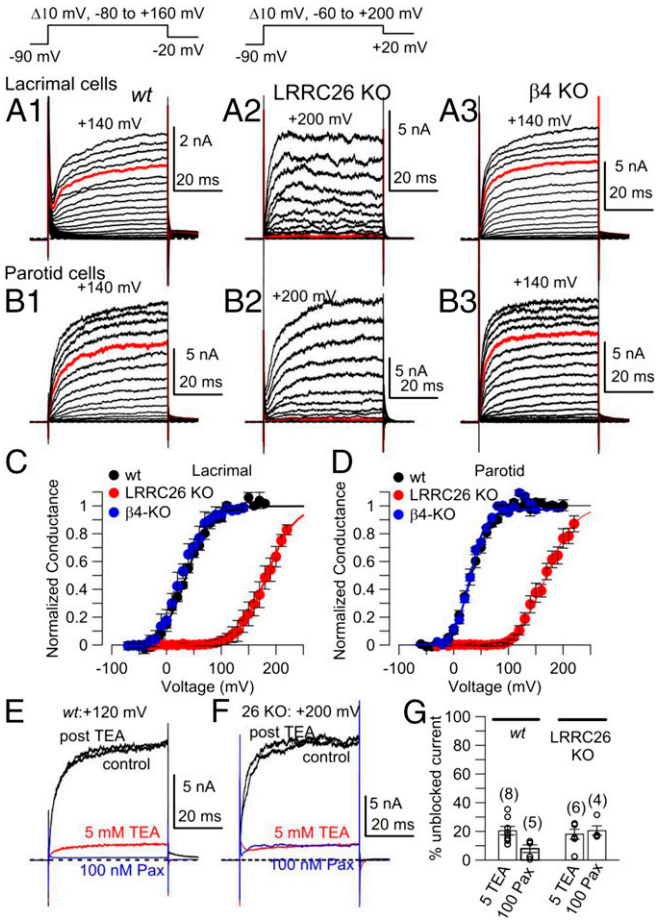

Fig. 4. KO of LRRC26 shifts gating of lacrimal gland and parotid cell BK currents rightward. (*A1*) Currents (shown to +140 mV) were activated with the indicated voltage protocol in a *wt* lacrimal gland cell. Pipette/intracellular Ca^{2+} was 250 nM for all whole-cell recordings. (*A2*) Currents are shown from a LRRC26 KO lacrimal gland cell with steps to +200 mV. (*A3*) Currents are shown up to +140 mV from a β4-KO lacrimal gland cell. For all panels in *A*, red traces are at +100 mV. (*B*) Panels on the *Left* (*B1*), *Middle* (*B2*), and *Right* (*B3*) correspond to currents from *wt*, LRRC26-KO, and β4-KO parotid gland cells, activated by voltage protocols identical to those in *A*. (*C*) GV curves were generated from tail currents in lacrimal gland cells from *wt* ($n = 4$), LRRC26 KO ($n = 4$), and β4 KO ($n = 3$). For *wt* and β4 KO, tail currents were measured at −20 mV, and for LRRC26-KO, +20 mV. V_h and z values from means of fits to individual cells are: for *wt*, $V_h = 36.7 \pm 1.4$ mV with $z = 1.2 + 0.1e$; for LRRC26 KO, $V_h = 182.2 \pm 9.5$ mV, $z = 1.1 \pm 0.1e$; for β4 KO, $V_h = 30.0 \pm 8.8$ mV, $z = 1.2 \pm 0.02e$. (*D*) GV curves were generated from tail currents in parotid cells as in *C*. From fits to individual cells, for 12 *wt* cells, mean $V_h = 33.5 \pm 1.5$ mV and $z = 1.6 \pm 0.1e$; for 12 LRRC26 KO cells, $V_h = 163.2 \pm 6.7$ mV with $z = 1.3 \pm 0.1e$. Fit of averaged GVs yielded similar values: for *wt*, $V_h = 33$ with $z = 1.3e$, and for LRRC26 KO, $V_h = 169.5$, with $z = 1.0e$. (*E*) Traces show inhibition at +120 mV (maximal BK activation) by 5 mM TEA and 100 nM paxilline (Pax) in a *wt* parotid cell. (*F*) Traces shown inhibition at +200 mV (maximal activation) by 5 mM TEA and 100 nM paxilline in a LRRC26 KO parotid cell. (*G*) The mean % of current remaining compared with control in 5 mM TEA or 100 nM paxilline is plotted for *wt* and LRRC26 KO parotid cells, with open circles corresponding to individual cells.

submandibular glands (30, 31). In one set of *wt* and LRRC26 KO animals, we used an in vivo assay to simultaneously collect from either the parotid or submandibular glands the fluid secretion induced by the muscarinic agonist, pilocarpine. This assay showed that, in the LRRC26 KO animals, K^+ concentration was reduced by about 50% in the saliva of both parotid (Fig. 5*A*) and submandibular (Fig. 5*B*) glands. The magnitude of these changes is comparable to those observed using the same assay in SLO1 KO mice (30, 31). In another set of *wt* and LRRC26 KO mice, the carbachol-evoked secretion from the submandibular gland was used in an ex vivo assay to assess effects on secretion independent of potential systemic effects of the agonist. In the ex vivo assay, the K^+ concentration in saliva secreted from the submandibular was reduced to a similar extent as observed in vivo (Fig. 5*B*). This decrease was comparable to earlier results in SLO1 KO mice (30, 31).

Discussion

The present results show that *Lrrc26* message and LRRC26 protein appear to be specifically associated with secretory epithelial cells, in some cases organized into acini, and most likely including both those secreting primarily fluid (serous) and those secreting mucus (mucous). This finding is supported by the distribution of *Lrrc26* message, the Bluo-Gal–defined loci of *Lrrc26* promoter activity, and the presence of verified LRRC26 protein in many relevant tissues. For three cases in which LRRC26 protein can be most readily detected: lacrimal gland, parotid gland, and colon, coimmunoprecipitation of LRRC26 protein with BK channel pore-forming subunits was demonstrated. Furthermore, in three cases: lacrimal, parotid, and submandibular glands, changes in BK channel properties in the LRRC26 KO animal reveal that BK channels in such *wt* cells are normally associated with LRRC26. The fact that LRRC26 is a normal part of BK channels has also previously been established for prostate tumor cells (12). Finally, we show that, in salivary gland, the previously established effect of BK channel KO on salivary K^+ concentration (30, 31) can be entirely mimicked by LRRC26 KO. Because of the remarkable left-shifted gating behavior of LRRC26-containing BK channels, we suggest that the activity of such BK channels near normal cell resting potentials plays a unique role in maintaining high K^+ fluxes that are essential to secretion in all secretory epithelial cells. At present, whether this is true in all cellular loci in which *Lrrc26* message and LRRC26 protein are found remains to be established. For those tissues for which we do not have functional data, e.g., trachea, bronchioles, small intestine, mammary gland, and uterine and vaginal epithelium, the present results only suggest that specific attention to the role of LRRC26-containing BK channels in the regulation of secretion in such cells is warranted.

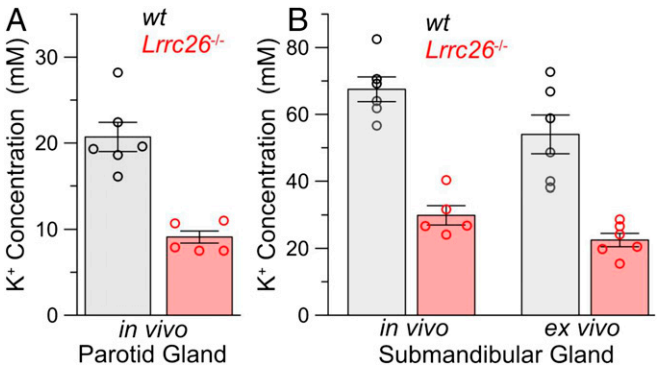

Fig. 5. LRRC26 KO mimics effect of SLO1 KO in reducing K^+ efflux in salivary gland secretions. (*A*) Potassium content was measured from pilocarpine-induced fluid secretion from in vivo parotid glands, for *wt* (gray) and LRRC26 KO animals. Height of bars shows mean with error bars indicating SEM, whereas circles show individual determinations. Each determination is the average of secretion measured separately from both glands in a single animal, except in one case where only a single gland was obtained. (*B*) Two bars on the left compare potassium content in submandibular gland saliva from an in vivo measurement, and the two bars on the right show ex vivo potassium content of submandibular salivary secretion. For all comparisons between *wt* and *Lrrc26*$^{-/-}$ glands in both *A* and *B*, $P < 0.001$ for the *t* test.

Loci of Expression of LRRC26-Containing BK Channels in Native Tissues. The marked diversity in BK channel properties among different cells depends in large measure on the identity of particular regulatory subunits in a given BK channel complex (15, 34). LRRC26-containing BK channels, with their enormously shifted activation range, are probably those BK channels most suited for unique roles in nonexcitable cells. Based on previous results and results reported here: Where have BK channels with properties consistent with the presence of LRRC26 subunits definitively been found?

Previous functional data have suggested the presence of LRRC26-containing BK channels in prostate tumor cells (12, 17) and parotid acinar cells (18, 19). Other tissues in which BK channels appear to be activated at unusually negative voltage ranges include lacrimal gland (2, 35) and pancreatic acinar cells (36). The present results confirm that the gating range of parotid, submandibular, and lacrimal gland BK channels is defined by LRRC26. There is also some pharmacological and functional evidence supporting the presence of LRRC26-containing BK channels in tracheal epithelium (37), based on the presence of a mallotoxin-resistant component of a BK-dependent process. Mallotoxin has been shown to be an activator of BK channels at low nanomolar concentrations (38), but heterologously expressed BK channels containing LRRC26 are resistant to mallotoxin as are the native BK channels in parotid (19). The specific identity of the tracheal cell type that participates in that phenomenon has not been identified. However, based on the distribution of Bluo-Gal staining, we propose that LRRC26-containing BK channels in the trachea are specifically located in the bronchiolar exocrine cells known as club cells and also goblet cells, but additional work will be required to clarify this. In regards to pancreas, although we detected low levels of *Lrrc26* message in pancreatic samples, we were unable to detect LRRC26 protein. Based on early recordings from pancreatic acinar cells (39, 40) in which half activation of BK channels occurred at very negative voltages, we think it likely that LRRC26-containing BK channels are present in such cells, albeit at low current density. In fact, probably the best criterion for the presence of LRRC26-containing BK channels in a given cell type will rest on demonstration of appreciable fractional activation of BK channels at membrane potentials negative to 0 mV with 0 cytosolic Ca^{2+}. When LRRC26 protein is clearly coassembled with BK channels, the extreme gating shift at 0 Ca^{2+} of such BK channels is unambiguous (28). LRRC26 has also been proposed to contribute to BK channels in brain arteriole smooth muscle (41), but BK channels and currents with the functional properties characteristic of those associated with LRRC26 subunits were not observed. Here we found no evidence for the presence of *Lrrc26* message or LRRC26 protein in various neuronal cells, electrically excitable endocrine cells, or aortic smooth muscle cells.

One other interesting cell type that exhibits BK currents with properties that seem indicative of the potential presence of LRRC26 subunits is that of hair cells of the cochlea. These cells are, in fact, epithelial-derived cells (42). In such cells, with 0 cytosolic Ca^{2+}, BK currents are activated at very negative potentials relative to other BK currents (43, 44), very similar to currents produced by the presence of LRRC26. Although this possibility will require further attention, we were unable to obtain any indication of *Lrrc26* message in the cochlea.

The Role of LRRC26 in Exocrine Gland Secretory Function and Epithelial Cell Function. Although the physiological role of LRRC26-containing BK channels in most tissues remains largely unaddressed, previous work has established that BK channels in parotid and submandibular glands are essential for normal secretory function. BK KO results in decreased K^+ concentrations in secreted fluid from mouse submandibular (31) and parotid (1) glands. The results here confirm that, in parotid, submandibular, and lacrimal gland, the shifted gating of BK channels in those cells arises from the presence of LRRC26, as originally suggested by Begenisich and colleagues in regards to parotid (18, 19). Here we tested the possibility that the simple absence of the LRRC26 subunit might be sufficient to mimic the effects of BK α-subunit KO. Consistent with this idea, we observed a decrease in concentration of secreted [K^+] from both the parotid and submandibular glands of LRRC26 KO animals similar to previous observations from SLO1 KO animals (1, 31). This observation supports the view that the presence of the LRRC26 subunit in BK channels in these cells is the key determinant that defines the physiological role of BK channels in maintaining normal secretion of K^+. We hypothesize that the presence of LRRC26-containing BK channels in other secretory epithelial cells will exert similar functional roles in maintaining secretory function.

The present results offer a number of intriguing hypotheses for future work. In the case of lacrimal glands, it would be expected that the [K^+] in the tears of LRRC26 KO mice would be reduced. Furthermore, in intestine and colon, given the importance of goblet and Paneth cells in maintaining the normal mucus layer and protection against bacterial infection (45, 46), it might be expected that LRRC26 KO mice may manifest gastrointestinal and colon dysfunctions with appropriate triggers. We anticipate that the LRRC26 KO mice will be useful in assessing important physiological roles of secretory epithelial cells in a variety of cells.

Potential Roles of LRRC26-Containing BK Channels in Tumor Growth Regulation. Before its recognition as a likely BK regulatory subunit, message and protein for human LRRC26 was initially observed in a variety of cancer cell lines and human cancer samples (CAPC) (16). CAPC was found to inhibit tumor cell proliferation and tumor growth by regulating NF-κB and its target genes (20). These observations raise two questions: First, is there a specific role of LRRC26-containing BK channels in tumor growth regulation and, second, might LRRC26 have functions unrelated to BK channels? Although the present findings are not adequate to answer these questions, in those tissues where we have directly recorded BK currents or tested for coassembly between LRRC26 and BK α-subunits, LRRC26 appears to be a critical regulatory component of BK channels. Given that a large number of ion channels have been implicated in tumor growth regulation, including KCa3.1 (47, 48), calcium channels (49), sodium channels (50), and a variety of K^+ channels (51, 52), these associations raise the possibility that specific ion channels per se may not be intrinsically related to tumor growth regulation, but that some aspect of membrane potential regulation, perhaps linked to cell cycle regulation, is the determinant of whether a given ion channel may promote or impede tumor growth.

Overview. The present results suggest that the large gating shift produced by LRRC26 serves specific physiological roles in a specific type of epithelial cell, perhaps related to the ability of LRRC26-containing BK channels to be activated near normal cell resting potentials at basal or low cytosolic Ca^{2+} levels (12). However, LRRC26 is one of a family of LRRC proteins, including LRRC52, LRRC38, and LRRC52, which together have been designated as a γ-subunit family (γ1–γ4) that associates with SLO family channels (14). Might other γ-subunits play equally specific roles in regulating BK channels in other loci? At present, only LRRC26 (γ1) can unambiguously be claimed to be a BK regulatory subunit in native tissues. Although all of the other γ-subunits appear competent to modestly shift BK gating when coexpressed with BK α-subunits in heterologous systems, this does not prove that such subunits contribute to BK channels in native tissues. At present, LRRC52 (γ2) appears to be exclusively expressed in mammalian sperm (13) and is a critical regulatory subunit of the alkalization-activated SLO3 K^+ channel (53), the closest homolog of the SLO1/BK channel. Specific interaction partners for LRRC38 and LRRC55 in native tissues have not been identified.

The results presented here highlight the important point that LRRC26-containing BK channels play a unique physiological role distinct from BK channels composed of other regulatory subunits, e.g., α+β2 channels in endocrine cells or neurons, α+β1 subunits in smooth muscle, or α+β4 subunits in various brain loci. We observed that the K^+ concentration of saliva arising from parotid and submandibular acinar cells is reduced in LRRC26 KO mice in a fashion identical to that resulting from complete SLO1 KO. Thus, LRRC26 is essential to defining the physiological role of BK channels in such cells. By providing a major pathway for K^+ efflux close to normal cell resting potentials even in the absence of increases in cytosolic Ca^{2+}, LRRC26-containing BK channels likely play similar roles in maintaining K^+ efflux in all secretory epithelial cells. Because of the markedly distinct functional properties of BK channels of different subunit composition, these results suggest that, in discussions of the physiological roles of BK channels, particular attention must be given to identifying the regulatory subunit composition and its biophysical effects on BK channels in any given cell type.

Materials and Methods

Animal Care. Animals were handled and housed according to the National Institutes of Health Committee on Laboratory Animal Resources guidelines. All experimental protocols were approved by the Institutional Animal Care and Use Committees of Washington University (protocol 20150258) and the National Institute of Dental and Craniofacial Research, National Institutes of Health (protocol ASP 16-802).

Source of *Lrrc26* KO Mice. The *Lrrc26* KO mouse strain used for this research project was created from ES cell clone 10167A-D5, generated by Regeneron Pharmaceuticals, Inc. and made into live mice by the KOMP Repository (https://www.komp.org) and the Mouse Biology Program (https://mbp.mousebiology.org) at the University of California, Davis. Methods used to create the Velocigene targeted alleles have been published (54). The Velocigene-targeted allele was replaced with *lacZ* and a floxed reporter cassette (ZEN-UB1-hyg) (velocigene.com/komp/detail/10167).

Parotid, Submandibular, and Lacrimal Gland Dissociations. Parotid cells were isolated following the enzymatic digestion protocol previously described (1). Briefly, after mice were killed by CO_2 inhalation, the parotid glands were carefully removed and placed in Eagle's minimum essential medium solution containing 1% BSA (Sigma) and 2 mM of L-glutamine (BSA-GLN-MEM). The parotid glands were minced ∼300 times with fine scissors and digested in this solution containing 0.01% trypsin and 0.5 mM EDTA, at 37 °C, for 5 min. Trypsin digestion was stopped by addition of 0.2% of trypsin inhibitor (Sigma T90003) and the tissue was further digested for another 20 min with 0.17 mg/mL of Liberase TL (Roche) dissolved in BSA-GLN-MEM containing 0.2% of trypsin inhibitor, at 37 °C, with constant stirring at very low speed. After 10 min of Liberase digestion, the cells were mechanically dispersed by pipetting three to four times and placed back at 37 °C. Then, the cells were washed with BSA-GLN-MEM and centrifuged at 800 × *g* for 1 min, repeating this washing step once. A final wash was performed using Eagle's minimum essential medium containing only 2 mM of glutamine (GLN-MEM). Then, after centrifugation the cells were suspended in GLN-MEM, plated on coverslips previously treated with poly-D-lysine, allowed to attach during at least 45 min, and then maintained at room temperature until used (usually within 3 h after dissociation). Individual coverslips were subsequently transferred to a recording chamber continuously perfused with extracellular solution for electrophysiological recordings. Lacrimal and submandibular gland cells were dissociated using a similar procedure with the following minor differences: Lacrimal gland dissociation omitted the initial trypsin treatment (Liberase treatment only), whereas submandibular glands required Liberase treatment for 30 min.

Basic Recording Methods. Standard whole-cell recording methods were done using an Axopatch 200B amplifier (Molecular Dynamics). Data acquisition was performed using a 16-bit analog/digital converter and voltage stimulation protocols were accomplished by using Clampex 8.0 (Molecular Dynamics) with analysis of waveforms done via Clampfit. Patch-clamp pipettes were made from borosilicate glass and coated with Sylgard. Typical pipette resistances after heat polishing typically were of 1.5–2.5 MΩ. Following whole-cell access, cells were used if the series resistance (R_s) was less than 10 GΩ. R_s was compensated 85%. Current records were filtered at 10 kHz. For whole-cell recordings, solutions were identical to those used in previous work on Ca^{2+}-dependent K^+ currents in parotid acinar cells in which extracellular and internal anions were largely replaced with glutamate, to remove contributions of any Cl^- currents (1). The bath solution (extracellular) consisted of (in millimoles): 135 Na-glutamate, 5 K-glutamate, 2 $CaCl_2$, 2 $MgCl_2$, 10 Hepes (pH 7.2). The pipette solution (intracellular) consisted of (in millimoles): 135 mM K-glutamate, 10 Hepes and, 5 mM EGTA + 3 mM Ca^{2+}, which results in a free Ca^{2+} solution of 250 nM (pH 7.2). For these nominal ionic gradients, $E_K = -84.5$ mV. Tetraethylammonium or paxilline was added to the external solutions at final concentrations given in the text. Experiments were done at room temperature, typically 22–24 °C.

In Vivo and ex Vivo Saliva Collection and [K^+] Determination. In vivo secretion was stimulated by i.p. injection of the cholinergic receptor agonist pilocarpine-HCl (10 mg/kg body weight) from mice anesthetized by i.p. injection of chloral hydrate (400 mg/kg body weight). Gland-specific ductal saliva was collected for 30-min stimulation by dissecting the ducts from the parotid and submandibular glands and inserting their distal ends into individual calibrated glass capillary tubes (Sigma-Aldrich). Body temperature was maintained at 37 °C using a regulated blanket (Harvard Apparatus). Ex vivo submandibular perfusion was performed at room temperature as previously reported (30). In brief, following ligation of all branches of the common carotid artery except the submandibular artery, the submandibular gland was removed, cannulated, perfused, and the main duct inserted into a calibrated glass capillary tube. Salivation was stimulated for 10 min by addition of the cholinergic receptor agonist carbachol (0.5 μM). The ex vivo perfusion solution contained (in millimoles): 4.3 KCl, 120 NaCl, 25 $NaHCO_3$, 5 glucose, 10 Hepes, 1 $CaCl_2$, 1 $MgCl_2$, pH 7.4. The saliva collected was stored at −20 °C. The potassium concentration was analyzed by atomic absorption spectroscopy (PerkinElmer Life Sciences 3030 spectrophotometer).

Statistical Analysis. The Kolmogorov–Smirnov (KS) test was used to generate the KS statistic, *P*. For cases in which the number of entries in one or both sample populations was less than 10, a two-tailed, unpaired Student's *t* test was used. Data are presented as mean ± SEM. Bar graphs for the K^+ secretion data display the mean and SE. Significance was determined using Student's *t* test with $P < 0.05$ considered to be statistically significant.

ACKNOWLEDGMENTS. We thank Ramon Lorca (University Colorado-Denver) for assistance in staging of pregnant females and Ted Begenisich for guidance and insightful comments on the nuances of salivary gland physiology. This work was supported in part by NIH Grant GM 118114 (to C.J.L.); NIH DE000738 from the Intramural Research Program of the National Institute of Dental and Craniofacial Research (NIDCR), National Institutes of Health (to J.E.M.); the Department of Anesthesiology; Washington University School of Medicine; the Intramural Research Program of the NIH–NIDCR; and the NIDCR Veterinary Research Core DE000740.

1. Romanenko V, Nakamoto T, Srivastava A, Melvin JE, Begenisich T (2006) Molecular identification and physiological roles of parotid acinar cell maxi-K channels. *J Biol Chem* 281:27964–27972.
2. Trautmann A, Marty A (1984) Activation of Ca-dependent K channels by carbamoylcholine in rat lacrimal glands. *Proc Natl Acad Sci USA* 81:611–615.
3. Linley J, Loganathan A, Kopanati S, Sandle GI, Hunter M (2014) Evidence that two distinct crypt cell types secrete chloride and potassium in human colon. *Gut* 63:472–479.
4. Barrett JN, Magleby KL, Pallotta BS (1982) Properties of single calcium-activated potassium channels in cultured rat muscle. *J Physiol* 331:211–230.
5. Adelman JP, et al. (1992) Calcium-activated potassium channels expressed from cloned complementary DNAs. *Neuron* 9:209–216.
6. Knaus HG, et al. (1994) Primary sequence and immunological characterization of beta-subunit of high conductance $Ca^{(2+)}$-activated K^+ channel from smooth muscle. *J Biol Chem* 269:17274–17278.
7. Xia X-M, Ding JP, Lingle CJ (1999) Molecular basis for the inactivation of Ca^{2+}- and voltage-dependent BK channels in adrenal chromaffin cells and rat insulinoma tumor cells. *J Neurosci* 19:5255–5264.
8. Wallner M, Meera P, Toro L (1999) Molecular basis of fast inactivation in voltage and Ca^{2+}-activated K^+ channels: A transmembrane beta-subunit homolog. *Proc Natl Acad Sci USA* 96:4137–4142.
9. Uebele VN, et al. (2000) Cloning and functional expression of two families of beta-subunits of the large conductance calcium-activated K^+ channel. *J Biol Chem* 275:23211–23218.
10. Weiger TM, et al. (2000) A novel nervous system beta subunit that downregulates human large conductance calcium-dependent potassium channels. *J Neurosci* 20:3563–3570.
11. Brenner R, Jegla TJ, Wickenden A, Liu Y, Aldrich RW (2000) Cloning and functional characterization of novel large conductance calcium-activated potassium channel beta subunits, hKCNMB3 and hKCNMB4. *J Biol Chem* 275:6453–6461.

12. Yan J, Aldrich RW (2010) LRRC26 auxiliary protein allows BK channel activation at resting voltage without calcium. *Nature* 466:513–516.
13. Yang C, Zeng XH, Zhou Y, Xia XM, Lingle CJ (2011) LRRC52 (leucine-rich-repeat-containing protein 52), a testis-specific auxiliary subunit of the alkalization-activated Slo3 channel. *Proc Natl Acad Sci USA* 108:19419–19424.
14. Yan J, Aldrich RW (2012) BK potassium channel modulation by leucine-rich repeat-containing proteins. *Proc Natl Acad Sci USA* 109:7917–22.
15. Latorre R, et al. (2017) Molecular determinants of BK channel functional diversity and functioning. *Physiol Rev* 97:39–87.
16. Egland KA, et al. (2006) High expression of a cytokeratin-associated protein in many cancers. *Proc Natl Acad Sci USA* 103:5929–5934.
17. Gessner G, et al. (2005) BKCa channels activating at resting potential without calcium in LNCaP prostate cancer cells. *J Membr Biol* 208:229–240.
18. Romanenko VG, Thompson J, Begenisich T (2010) Ca^{2+}-activated K channels in parotid acinar cells: The functional basis for the hyperpolarized activation of BK channels. *Channels (Austin)* 4:278–288.
19. Almassy J, Begenisich T (2012) The LRRC26 protein selectively alters the efficacy of BK channel activators. *Mol Pharmacol* 81:21–30.
20. Liu XF, et al. (2012) CAPC negatively regulates NF-κB activation and suppresses tumor growth and metastasis. *Oncogene* 31:1673–1682.
21. Karam SM (1999) Lineage commitment and maturation of epithelial cells in the gut. *Front Biosci* 4:D286–D298.
22. van Es JH, et al. (2005) Notch/gamma-secretase inhibition turns proliferative cells in intestinal crypts and adenomas into goblet cells. *Nature* 435:959–963.
23. Bergstrom KS, et al. (2008) Modulation of intestinal goblet cell function during infection by an attaching and effacing bacterial pathogen. *Infect Immun* 76:796–811.
24. Lee G, White LS, Hurov KE, Stappenbeck TS, Piwnica-Worms H (2009) Response of small intestinal epithelial cells to acute disruption of cell division through CDC25 deletion. *Proc Natl Acad Sci USA* 106:4701–4706.
25. Katz S, Merzel J (1977) Distribution of epithelia and glands of the nasal septum mucosa in the rat. *Acta Anat (Basel)* 99:58–66.
26. Gipson IK (2016) Goblet cells of the conjunctiva: A review of recent findings. *Prog Retin Eye Res* 54:49–63.
27. Odaka A, et al. (2012) Efficacy of retinol palmitate eye drops for dry eye in rabbits with lacrimal gland resection. *Clin Ophthalmol* 6:1585–1593.
28. Gonzalez-Perez V, Xia XM, Lingle CJ (2014) Functional regulation of BK potassium channels by γ1 auxiliary subunits. *Proc Natl Acad Sci USA* 111:4868–4873.
29. Almassy J, Won JH, Begenisich TB, Yule DI (2012) Apical Ca^{2+}-activated potassium channels in mouse parotid acinar cells. *J Gen Physiol* 139:121–133.
30. Romanenko VG, Nakamoto T, Srivastava A, Begenisich T, Melvin JE (2007) Regulation of membrane potential and fluid secretion by Ca^{2+}-activated K^+ channels in mouse submandibular glands. *J Physiol* 581:801–817.
31. Nakamoto T, Romanenko VG, Takahashi A, Begenisich T, Melvin JE (2008) Apical maxi-K (KCa1.1) channels mediate K^+ secretion by the mouse submandibular exocrine gland. *Am J Physiol Cell Physiol* 294:C810–C819.
32. Nehrke K, Quinn CC, Begenisich T (2003) Molecular identification of Ca^{2+}-activated K^+ channels in parotid acinar cells. *Am J Physiol Cell Physiol* 284:C535–C546.
33. Meera P, Wallner M, Toro L (2000) Molecular basis of charybdotoxin and iberiotoxin insensitive MaxiK channels: A novel β subunit. *Biophys J* 78:91A.
34. Hoshi T, Pantazis A, Olcese R (2013) Transduction of voltage and Ca^{2+} signals by Slo1 BK channels. *Physiology (Bethesda)* 28:172–189.
35. Marty A, Tan YP, Trautmann A (1984) Three types of calcium-dependent channel in rat lacrimal glands. *J Physiol* 357:293–325.
36. Petersen OH, Maruyama Y (1984) Calcium-activated potassium channels and their role in secretion. *Nature* 307:693–696.
37. Manzanares D, et al. (2014) IFN-γ-mediated reduction of large-conductance, Ca2+-activated, voltage-dependent K+ (BK) channel activity in airway epithelial cells leads to mucociliary dysfunction. *Am J Physiol Lung Cell Mol Physiol* 306:L453–L462.
38. Zakharov SI, Morrow JP, Liu G, Yang L, Marx SO (2005) Activation of the BK (SLO1) potassium channel by mallotoxin. *J Biol Chem* 280:30882–30887.
39. Maruyama Y, Petersen OH, Flanagan P, Pearson GT (1983) Quantification of Ca^{2+}-activated K^+ channels under hormonal control in pig pancreas acinar cells. *Nature* 305:228–232.
40. Petersen OH (1986) Calcium-activated potassium channels and fluid secretion by exocrine glands. *Am J Physiol* 251:G1–G13.
41. Evanson KW, Bannister JP, Leo MD, Jaggar JH (2014) LRRC26 is a functional BK channel auxiliary γ subunit in arterial smooth muscle cells. *Circ Res* 115:423–431.
42. Forge A, Wright T (2002) The molecular architecture of the inner ear. *Br Med Bull* 63: 5–24.
43. Pyott SJ, Glowatzki E, Trimmer JS, Aldrich RW (2004) Extrasynaptic localization of inactivating calcium-activated potassium channels in mouse inner hair cells. *J Neurosci* 24:9469–9474.
44. Thurm H, Fakler B, Oliver D (2005) Ca^{2+}-independent activation of BKCa channels at negative potentials in mammalian inner hair cells. *J Physiol* 569:137–151.
45. Pelaseyed T, et al. (2014) The mucus and mucins of the goblet cells and enterocytes provide the first defense line of the gastrointestinal tract and interact with the immune system. *Immunol Rev* 260:8–20.
46. Birchenough GM, Johansson ME, Gustafsson JK, Bergström JH, Hansson GC (2015) New developments in goblet cell mucus secretion and function. *Mucosal Immunol* 8: 712–719.
47. Turner KL, Honasoge A, Robert SM, McFerrin MM, Sontheimer H (2014) A proinvasive role for the Ca(2+) -activated K(+) channel KCa3.1 in malignant glioma. *Glia* 62: 971–981.
48. Bonito B, Sauter DR, Schwab A, Djamgoz MB, Novak I (2016) KCa3.1 (IK) modulates pancreatic cancer cell migration, invasion and proliferation: Anomalous effects on TRAM-34. *Pflugers Arch* 468:1865–1875.
49. Buchanan PJ, McCloskey KD (2016) CaV channels and cancer: Canonical functions indicate benefits of repurposed drugs as cancer therapeutics. *Eur Biophys J* 45: 621–633.
50. Nelson M, Yang M, Millican-Slater R, Brackenbury WJ (2015) Nav1.5 regulates breast tumor growth and metastatic dissemination in vivo. *Oncotarget* 6:32914–32929.
51. Comes N, et al. (2015) Involvement of potassium channels in the progression of cancer to a more malignant phenotype. *Biochim Biophys Acta* 1848:2477–2492.
52. Huang X, Jan LY (2014) Targeting potassium channels in cancer. *J Cell Biol* 206: 151–162.
53. Zeng XH, Yang C, Xia XM, Liu M, Lingle CJ (2015) SLO3 auxiliary subunit LRRC52 controls gating of sperm KSPER currents and is critical for normal fertility. *Proc Natl Acad Sci USA* 112:2599–2604.
54. Valenzuela DM, et al. (2003) High-throughput engineering of the mouse genome coupled with high-resolution expression analysis. *Nat Biotechnol* 21:652–659.